Research Article

Dianlun Li#, Lu Ruan#, Jie Sun*, Chaoxing Wu*, Ziwen Yan, Jintang Lin, and Qun Yan

Facile growth of aluminum oxide thin film by chemical liquid deposition and its application in devices

https://doi.org/10.1515/ntrev-2020-0062
#received January 16, 2020; accepted January 24, 2020

Abstract: Uniform and continuous Al_2O_3 thin films were prepared by the chemical liquid deposition (CLD) method. The breakdown field strength of the amorphous CLD-Al_2O_3 film is 1.74 MV/cm, making it could be used as a candidate dielectric film for electronic devices. It was further proposed to use the CLD-Al_2O_3 film as an electron blocking layer in a triboelectric nanogenerator (TENG) for output performances enhancement. Output voltages and currents of about 200 V and 9 μA were obtained, respectively, which were 2.6 times and 3 times, respectively, higher than TENG device without an Al_2O_3. A colloidal condensation-based procedure controlled by adjusting the pH value of the solution was proposed to be the mechanism of CLD, which was confirmed by the Tyndall effect observed in the growth liquid. The results indicated that the CLD could serve as a low-cost, room temperature, nontoxic and facile new method for the growth of functional thin films for semiconductor device applications.

Keywords: aluminum oxide, chemical liquid deposition, dielectric thin film, triboelectric nanogenerator

1 Introduction

Al_2O_3 is a functional material with good electrical insulation, large forbidden band width ($E_g \approx 8.8$ eV), high transparency, high refractive index, large mechanical strength, and good thermal conductivity [1–8]. It has stable chemical properties at high temperature. Al_2O_3 has a dielectric constant of about 8–10, which is more than twice as high as SiO_2. Al_2O_3 is also superior to SiO_2 and silicon nitride in its ability to resist radiation and to block impurities such as sodium ions [9]. It is more resistant to various acids and base corrosion compared to SiO_2. Therefore, Al_2O_3 could be used as an excellent dielectric and passivation layer in semiconductor electronic devices.

Currently, standard Al_2O_3 film preparation processes primarily comprise electron beam evaporation [10], magnetron sputtering [11], atomic layer deposition (ALD) [12], and plasma-enhanced chemical vapor deposition (PECVD) [13]. Even though Al_2O_3 films prepared by these methods are typically of high quality, these methods are complicated in process and generally require growth of the film under high temperature and vacuum conditions relying on very expensive equipment.

In this article, we introduce a simple and low-cost method that uses nontoxic liquid precursors to grow the Al_2O_3 film. It is named as chemical liquid deposition (CLD), in parallel with the commonly known chemical vapor deposition method. The thin film growth setup was simple, inexpensive, and easy to operate. Al_2O_3 thin films were prepared on the surface of Si substrates and indium tin oxide (ITO)-coated glasses (i.e., ITO glass) under ambient pressure and room temperature conditions. The deposition had the characteristics of uniform film growth on the substrate. The surface morphology, structural composition, electrical properties, and passivation properties of Al_2O_3 films prepared by the CLD method (CLD-Al_2O_3) were characterized by comprehensive material analysis. Triboelectric nanogenerators (TENGs) are a new type of simple and low-cost energy harvesting devices that could effectively convert various

# These authors contributed equally.

* **Corresponding author: Jie Sun,** Fujian Science & Technology Innovation Laboratory for Optoelectronic Information of China, and Optoelectronics Department, College of Physics and Information Engineering, Fuzhou University, Fuzhou, 350100, China, e-mail: jie.sun@fzu.edu.cn
* **Corresponding author: Chaoxing Wu,** Fujian Science & Technology Innovation Laboratory for Optoelectronic Information of China, and Optoelectronics Department, College of Physics and Information Engineering, Fuzhou University, Fuzhou, 350100, China, e-mail: nnnwcx@foxmail.com
Dianlun Li, Lu Ruan, Ziwen Yan, Jintang Lin, Qun Yan: Fujian Science & Technology Innovation Laboratory for Optoelectronic Information of China, and Optoelectronics Department, College of Physics and Information Engineering, Fuzhou University, Fuzhou, 350100, China

daily wasted mechanical energy into electric energy by utilizing triboelectric charging and electrostatic induction effects [14–17]. As an example of the device application, we used CLD-Al_2O_3 as an electron-blocking layer in TENG, which effectively prevented charge leakage during operation and enhanced the output performance of TENG. Experiments showed that the output performance of the TENG with the Al_2O_3 blocking layer was significantly improved compared to the conventional TENG structure. In addition, the electron blocking layer located at the bottom of the friction layer provided a long-term performance enhancement for TENG. Finally, through the observation of the Tyndall effect, we had revealed that the growth mechanism of the CLD method was essentially a colloidal condensation process caused by adjusting the pH value. Note that this mechanism should not be confused with the traditional sol–gel method. Our results are important for the theoretical interpretation of CLD and could be used as the guideline for the design of CLD of other functional materials.

2 Materials and methods

2.1 Preparation of Al_2O_3 thin films by CLD

The chemical reagents used in this experiment were purchased from Sinopharm Chemical Reagent Co., Ltd. Figure 1a shows a schematic process for the Al_2O_3-CLD, and the specific preparation procedures are as follows:

(1) $Al_2(SO_4)_3{\cdot}18H_2O$ (50 g) was dissolved in 50 mL of deionized (DI) water at room temperature. The solution was filtered (maximum pore size 15 μm) to remove few undissolved large particles and to obtain 73.25 mL colorless viscous liquid, whose nominal pH is about −0.26.

(2) The prepared $Al_2(SO_4)_3{\cdot}18H_2O$ solution was poured into a beaker and stirred using a magnetic stirrer, and 16.115 g of $NaHCO_3$ powder was slowly added into the solution. Each time when the $NaHCO_3$ was added, it was necessary to wait for the CO_2 foam to substantially disappear before continuing to add more. A small amount of residual $NaHCO_3$ pellets were treated with an ultrasonic device to dissolve them thoroughly to obtain 74.72 mL of a colorless transparent viscous liquid, whose pH was about 2.89. This liquid was prone to produce aluminum–sodium vanadium, so it should not be placed for a long time.

(3) The as-prepared liquid was immediately diluted with water by a volume ratio of 1:1, and the suspended residual matter in the liquid was filtered out, thereby obtaining 149.43 mL of colorless transparent liquid. Now the pH value is about 3.35.

(4) This liquid was further diluted with water with a volume ratio of 1:5 to obtain 896.58 mL of the growth liquid, whose pH was about 3.74. The Si substrates or ITO glasses were ultrasonically washed in acetone, absolute ethanol, and DI water for 10 min each and then dried. After the cleaning was completed, the surface was treated with oxygen

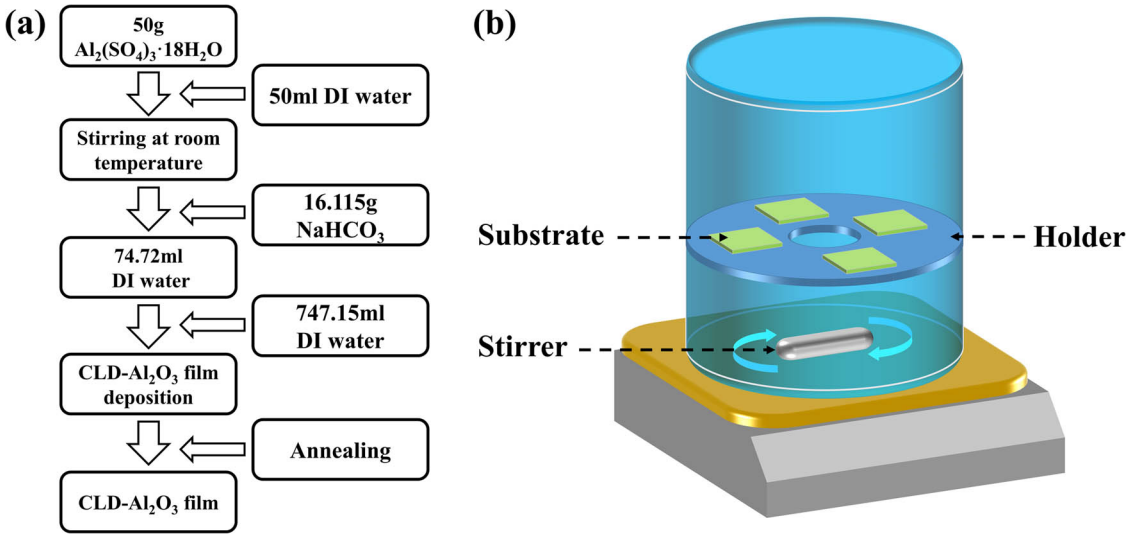

Figure 1: Illustration of the preparation of CLD-Al_2O_3 films. (a) Process flow chart for preparing Al_2O_3 thin films by the CLD method. (b) Schematic diagram of the Al_2O_3 growth setup.

plasma for 15 min to obtain some degree of hydrophilicity, so that a large amount of surface hydroxyl groups (OH groups) were decorated on the surface, which were advantageous for enhancing the chemical adsorption of the film material to the substrates. The samples were then placed on the surface of a Teflon stent in a Teflon beaker and immersed in the growth liquid, as shown in Figure 1b. The liquid was agitated with a magnetic stirrer at 200 rpm. After few hours at room temperature, the growth liquid eventually turned little turbid. The samples were taken out, cleaned with DI water, and dried in an oven at 60°C.

(5) Finally, the as-prepared samples were thermally annealed optional at 400°C for 1 h using a muffle furnace (heating rate 1.5°C/min) and were taken out after natural cooling.

2.2 Fabrication process of the TENG device with Al_2O_3 electron blocking layer

The TENG device consisted of a polydimethylsiloxane (PDMS)/Al_2O_3/ITO complex film and an Al metal layer operating in a vertical contact-separation mode [18]. PDMS (Sylgard 184, Dow Corning) base and a curing agent were mixed at a mass ratio of 10:1 and were spin coated at 3,000 rpm for 30 s onto the Al_2O_3-coated ITO glass. The PDMS was then cured at 150°C for 10 min. PDMS and Al act as negative and positive friction layers, respectively. The surfaces (contact area: $2 \times 2\,cm^2$) of the PDMS and Al film were periodically contacted and separated to generate a potential difference.

2.3 Measurement and characterization

The chemical compositions of the samples were analyzed by energy-dispersive spectroscopy (EDS, AMETEK) and X-ray photo-electron spectroscopy (XPS, Thermo Scientific, ESCALAB 250). The morphology of the Al_2O_3 films was characterized by ultra-high resolution field emission scanning electron microscopy (SEM, Thermo Scientific, Verios G4 UC) and atomic force microscopy (AFM, Bruker, Multimode 8). The crystal structure analysis of the Al_2O_3 films was performed using X-ray diffraction (XRD, Empyrean, DY1602). The thickness and the refractive index of the Al_2O_3 films were measured using ellipsometry (J.A. Woollam, M2000). The breakdown voltage of the film was measured by the semiconductor characterization system (Keithley, 4200). A signal generator (RIGOL, DG4162), a power amplifier (SINOCERA, YE5872A), and a vibration exciter (SINOCERA, JKZ-10) were combined to form a controllable tapping system to drive the TENG to work with the same external force and frequency. An oscilloscope (RIGOL, DS1102E) was used to record the voltage signal of the TENG output. The output current and the transferred charge were measured by using an electrometer (Keithley, 6514).

3 Results and discussion

The double hydrolysis reaction of $Al_2(SO_4)_3$ and $NaHCO_3$ in the experiment is given as follows:

$$\Delta H + Al_2(SO_4)_3 + 6NaHCO_3 = 2Al(OH)_3 + 3Na_2SO_4 + 6CO_2,$$

where $Al(OH)_3$ is actually $xAl_2O_3{\cdot}yH_2O$ and ΔH is the chemical reaction enthalpy ($\Delta H > 0$). $Al(OH)_3$ is a typical amphoteric hydroxide, which is soluble not only in strong acids but also in strong bases to form hydroxyl complexes. The solubility of $Al(OH)_3$ has a certain relationship with the pH value. $Al(OH)_3$ can be dissolved in the acidic environment with pH < 3.4 or an alkaline environment with pH > 12.9, and it does not substantially dissolve in the pH rang of 4–11.

In this experiment, a very high concentration of $Al_2(SO_4)_3$ solution was first prepared, and the solution exhibited strong acidity due to the hydrolysis of $Al_2(SO_4)_3$. After slowly adding an appropriate amount of $NaHCO_3$ powder, the $Al(OH)_3$ nominally formed by the double hydrolysis reaction will then all "dissolve" in the still strongly acidic liquid. However, Na_2SO_4, one of the reaction products, could form a double-salt aluminum–sodium vanadium ($NaAl(SO_4)_2{\cdot}12H_2O$) with $Al_2(SO_4)_3$. As aluminum–sodium vanadium could easily crystallize, it was necessary to dilute the liquid with water rapidly after the reaction of $Al_2(SO_4)_3$ with $NaHCO_3$ was completed. Then, the added water (volume ratio 1:1) had adjusted the pH to 3.35, very close to the critical value. This liquid was chemically relatively stable and could be stored if necessary (not more than a few weeks). Just before the film growth, DI water with five times the volume of the liquid was poured into the liquid to adjust the pH to 3.74, which was greater than the critical value of 3.4. At this point, the $Al(OH)_3$ in the liquid gradually precipitated onto the sample to initiate the nucleation and the

subsequent film formation. The surface was therefore deposited with a layer of $Al(OH)_3$ film, which was then annealed to eliminate the possibly existing H element, although this step was usually optional, since the amount of H is negligible.

3.1 Characterization of Al_2O_3 thin films grown by CLD

Figure 2a and b are AFM images of the CLD-Al_2O_3 film on Si substrate with a scan range of $4 \times 4\ \mu m^2$, and the AFM images of the corresponding Si substrate are shown in Figure 2c and d. The root-mean-square (RMS) surface roughness of the CLD-Al_2O_3 film and bare Si substrate was measured to be 0.068 and 0.232 nm, respectively. It shows that the surface of Al_2O_3 film is smooth and uniform, without obvious protrusions and holes. Figure 3a and the inset are SEM images of the Al_2O_3 film observed at magnifications of 1,00,000 and 2,00,000, respectively. This figure also shows that the surface morphology of the Al_2O_3 film is continuous, relatively flat, and uniform, with a few bumps occasionally. Generally, an insulating layer with the smooth surface is favorable for forming good interface contact with electron devices, which can improve the electrical performance and the stability of the devices [19].

Because the Al_2O_3 film was very thin, we did not detect any signal in the small incident angle XRD measurement [20]. Therefore, we performed XRD tests on the precipitate collected in the growth liquid instead, because the precipitate had exactly the same composition and structure as the film. The precipitate was filtered out from the growth liquid that had grown for 12 h, washed, dried, and annealed in a muffle furnace at 1,000°C for 1 h. The XRD curve was compared with the JCPDS card (46-1212 [21]) and confirmed as α-Al_2O_3, as shown in Figure 3b. We also characterized the powder annealed at 500°C but did not obtain conclusive results indicating a crystallization. Therefore, increasing the annealing temperature can indeed crystallize this

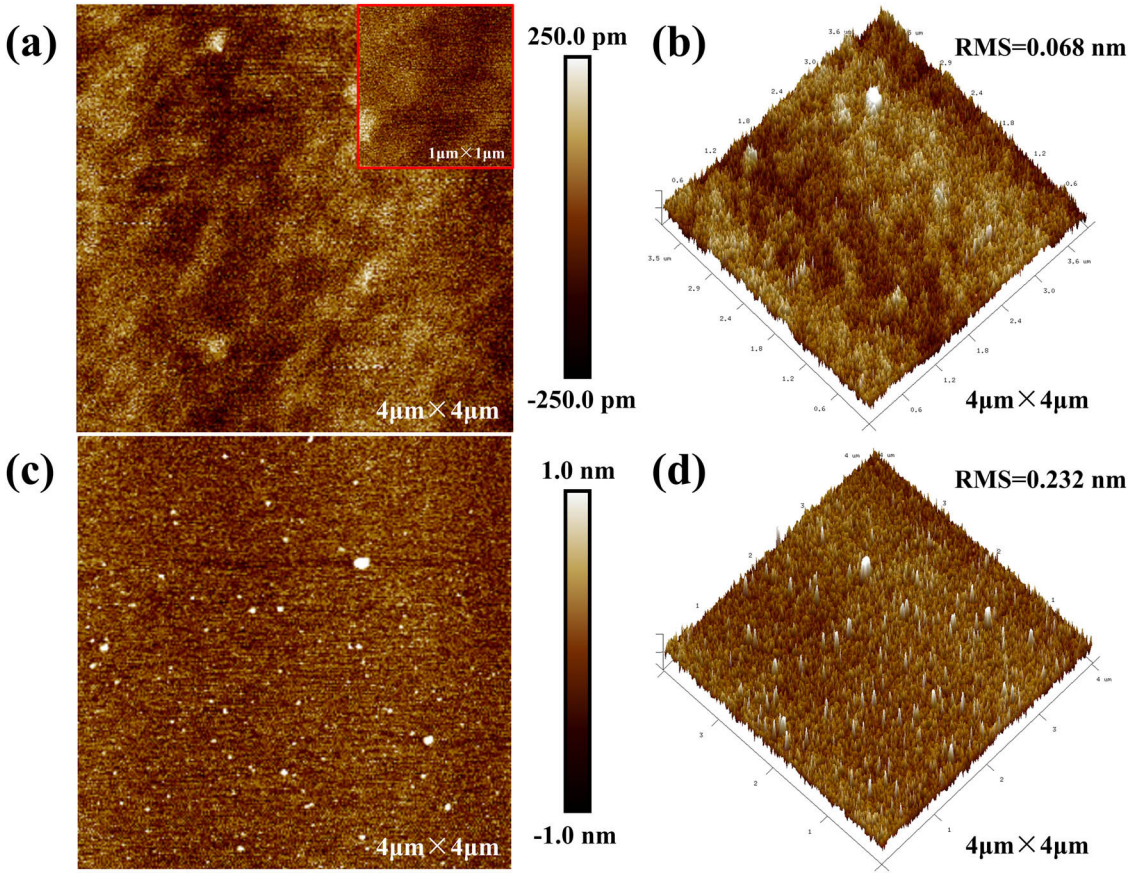

Figure 2: AFM micrographs of the CLD-Al_2O_3 and the Si substrate. (a) 2D and (b) 3D AFM images of the CLD-Al_2O_3 thin film on Si substrate. The inset is an AFM image with much higher magnification. (c) 2D and (d) 3D AFM images of the bare Si substrate.

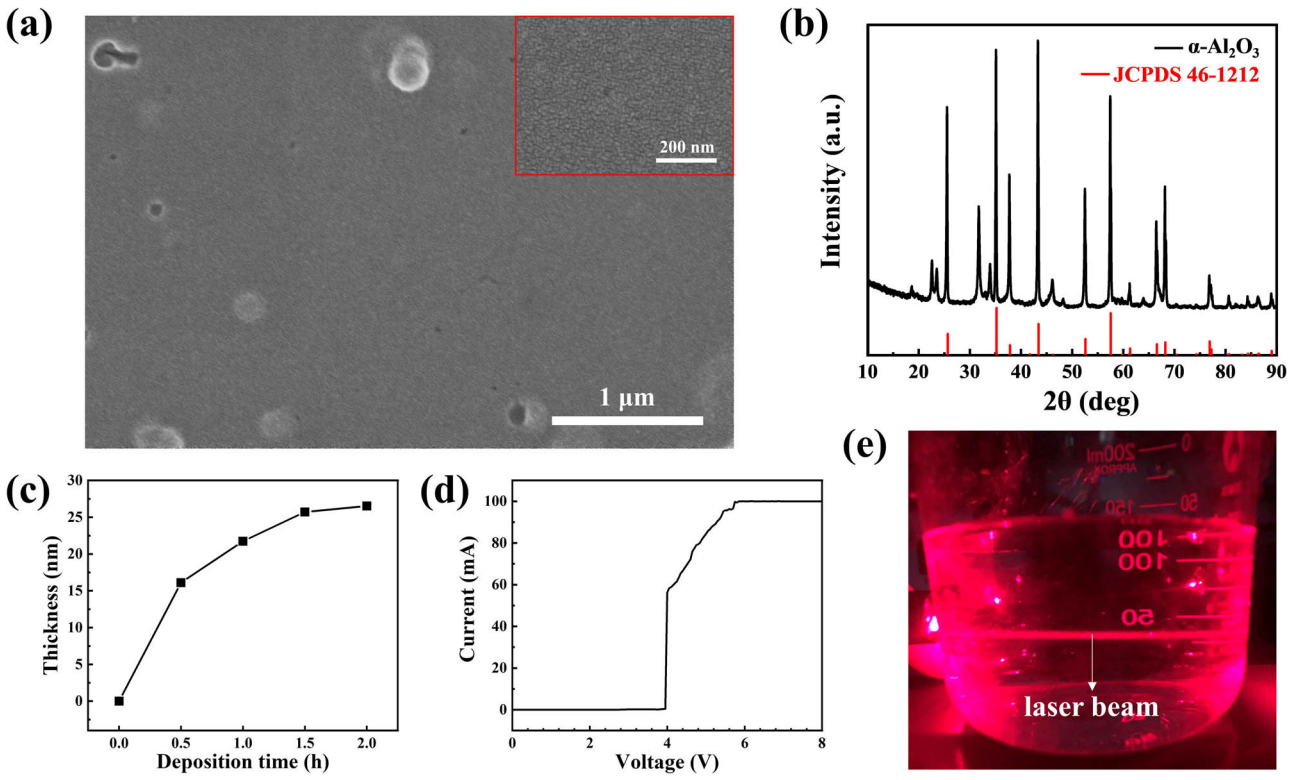

Figure 3: Material characterizations of the CLD-Al_2O_3. (a) SEM image of the CLD-Al_2O_3 thin film on ITO glass. The inset is an SEM image with much higher magnification where no features other than a continuous and flat film have been detected. (b) XRD curve of the CLD-Al_2O_3 (1,000°C annealing). (c) Deposition thickness of the CLD-Al_2O_3 film as a function of the growth time. (d) *I–V* characteristics of the 23 nm CLD-Al_2O_3 thin film sandwiched between two electrodes. The electrical breakdown occurs at ~4 V. (e) The Tyndall effect observed in the 1:1 diluted liquid. The horizontal laser beam is clearly visible.

material. However, for most applications in electronic devices, this crystallization is unnecessary. In general, films with an amorphous structure are isotropic, and their insulation and other properties are usually more uniform than the polycrystalline counterpart. In addition, the amorphous structure usually makes the surface of the dielectric layer flatter. If the film has a polycrystalline structure, the grain boundaries will become channels for impurity scattering and leakage current. The anisotropy will reduce the dielectric stability of the film. Furthermore, the grain boundary will increase the surface roughness of the film, increase the density of defect states at the interface with which the semiconductor layer is in contact, and directly affect the application of the dielectric film.

Several ITO glass substrates were simultaneously immersed in the growth liquid, and one sample was taken out every half an hour. After annealing at high temperature, the thickness and the refractive index of the grown Al_2O_3 films were measured by ellipsometry. The relation between the thickness and the growth time is shown in Figure 3c. It can be seen from the figure that the deposition rate is faster in the range of 0–0.5 h, which is about 32 nm/h. As the growth time increases, the growth rate of the film decreases, and it remains nearly constant at about 10 nm/h at 0.5–1.5 h. When the growth time exceeds 1.5 h, the film thickness remains almost unchanged, indicating that the liquid has already substantially lost its growth ability.

Figures 4a and b show the EDS spectrum of the Al_2O_3 film grown on the ITO surface and Si substrate (with a scan range of 0 to 5 keV, 400°C annealing), respectively. This figure also shows that there are clear O and Al signals at 0.53 and 1.49 keV, respectively. Apart from the In peak, there are no additional peaks detected, which indicates that the chemical composition of the CLD-Al_2O_3 film method is very pure. According to the peak values in Figure 4a, it can be quasi quantitatively inferred that the atomic ratio of the O element to the Al element is about 7:1, which deviates from the expected 3:2 ratio. The main reason is that the thickness of the Al_2O_3 film is small. A large amount of O element contained in the thick ITO film on the base surface is inevitably detected, so that the content of the O element appears significantly larger.

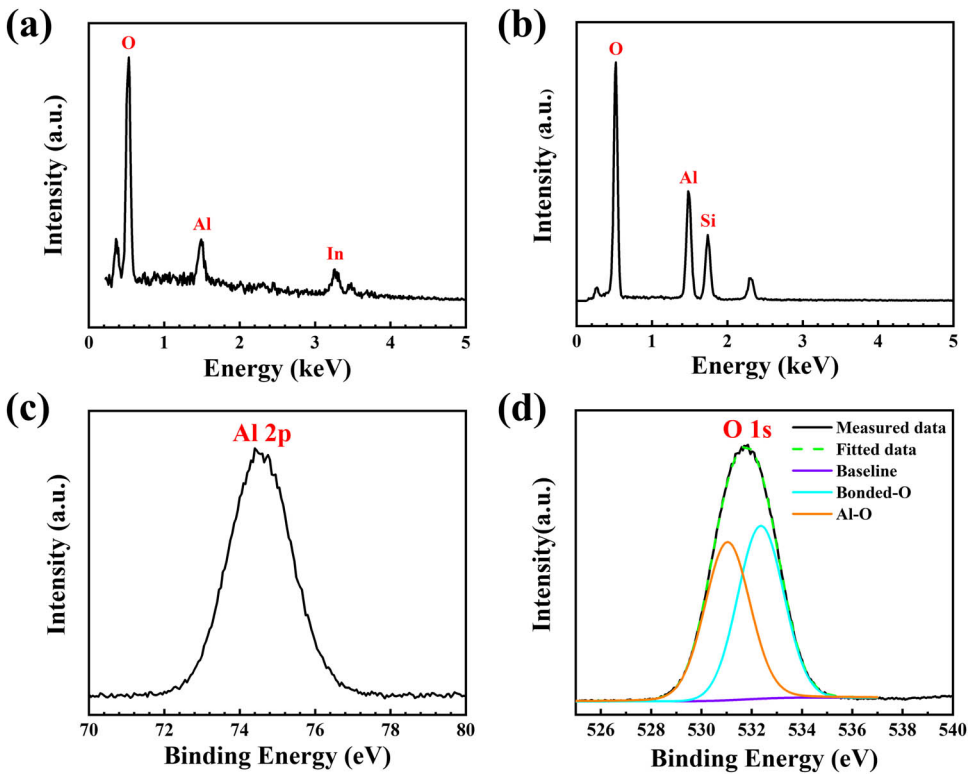

Figure 4: Elemental analysis of the CLD-Al_2O_3. EDS spectra of the CLD-Al_2O_3 on (a) ITO and (b) silicon after annealing at 400°C. XPS (c) Al 2p and (d) O 1s spectra of CLD-Al_2O_3 after annealing at 400°C.

The chemical composition of the CLD-Al_2O_3 film on the Si substrate (400°C annealing) was investigated by XPS measurements as well. In Figure 4c, the XPS spectrum shows a singlet Al 2p peak at 74.4 eV, which is consistent with the peak position of the oxidation state Al in the literature [22]. The XPS O 1s peak of the CLD-Al_2O_3 film is shown in Figure 4d. The black solid line shows the measured data, and the green dotted line represents the Gaussian peak fitting result. The O 1s peak in spectrum is deconvoluted into two sub-peaks corresponding to O^{2-} bonded with Al^{3+} ions in the Al_2O_3 film and oxygen associated with the OH^- in aluminum hydroxide, whose centers are located at around 531.05 and 532.35 eV, respectively [23]. It is worth noting that the associated OH groups are mainly due to water absorbed from the environment in the Al_2O_3 film [22].

3.2 Output performance of the TENG with CLD-Al_2O_3 layer

We applied the CLD-Al_2O_3 thin film in TENG as an electron blocking layer to enhance the output performance. At the same time, we also fabricated TENG without Al_2O_3 as a reference sample. The fabrication process is described in detail in the experimental section, and Figure 5a schematically shows the TENG with an Al_2O_3 film between the PDMS friction layer and the bottom electrodes. The cross-sectional SEM image of an Al_2O_3/ITO glass sample is shown in Figure 5b, where the Al_2O_3 film is about 260 nm thick. The TENG devices operate in a vertical contact-separation mode. The open circuit voltage, short circuit current, and amount of transferred charge amount of these devices are measured under the same applied force and frequency, as shown in Figures 5c–e. In Figure 5c, the open circuit voltage of the Al_2O_3-TENG is about 200 V, which is nearly 2.6 times that of the Al_2O_3-free TENG's open circuit voltage. The short circuit current also increases from about 3 to 9 μA, which is three times that of the TENG without Al_2O_3, as illustrated in Figure 5d. Meanwhile, the amount of transferred charge in the TENG with an Al_2O_3 layer is about 2.4 times higher than that of the TENG without Al_2O_3 (see Figure 5e).

Figures 6a–d schematically illustrates the principle of the Al_2O_3 electron blocking layer enhancing the TENG output performance. After several contact and

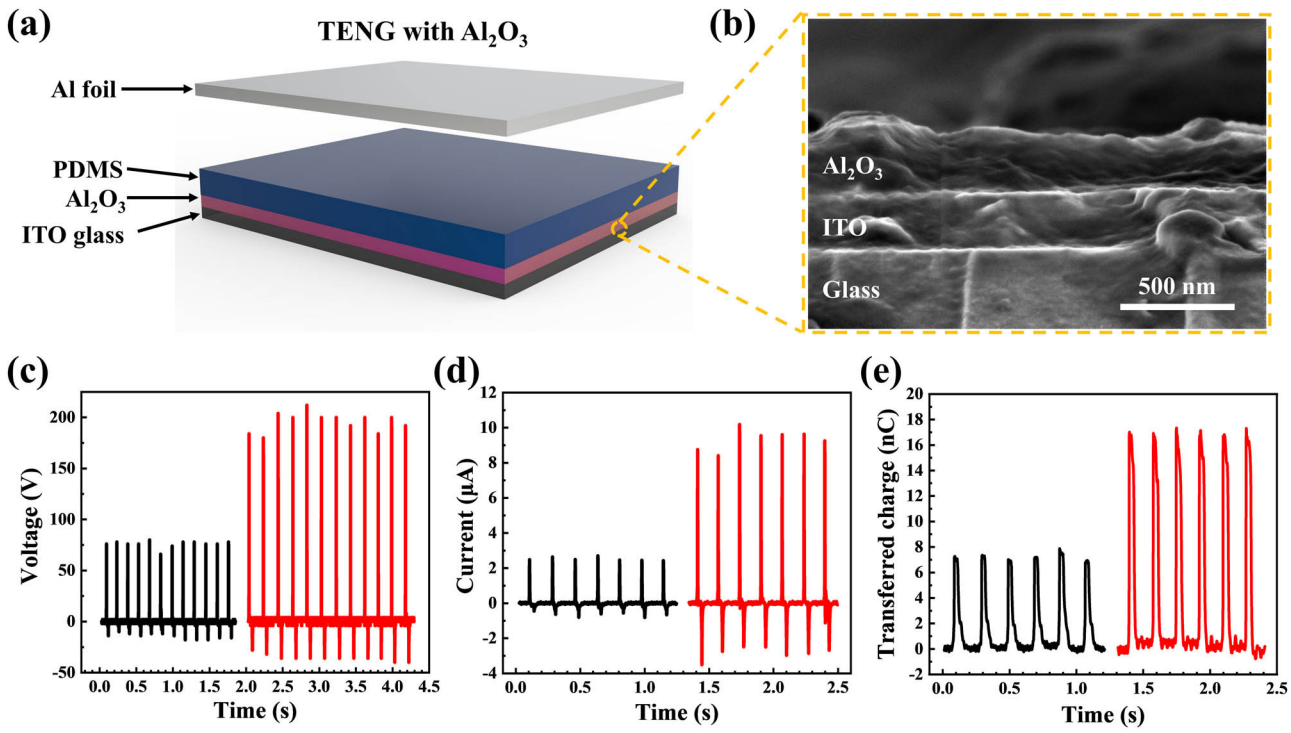

Figure 5: Device structure and performance of the TENG with CLD-Al_2O_3 layer. (a) Schematic diagram of the TENG device with the Al_2O_3 layer. (b) A cross-sectional view of SEM image of the Al_2O_3/ITO glass sample showing the sharp interfaces between different materials. (c) Open-circuit voltage of the TENG without (black)/with (red) the Al_2O_3 layer. (d) Short-circuit current of the TENG without (black)/with (red) the Al_2O_3 layer. (e) The amount of transferred charge of TENG without (black)/with (red) Al_2O_3.

separation cycles, the friction generated electrons are accumulated on the surface of the PDMS friction layer. At the same time, the bottom electrode will be positively charged due to electrostatic induction, so an electric field will be generated between the contact surface and the bottom electrode (the direction of the field is upward), as shown in Figure 6a. At this moment, there are two electron transfer procedures: a drift process

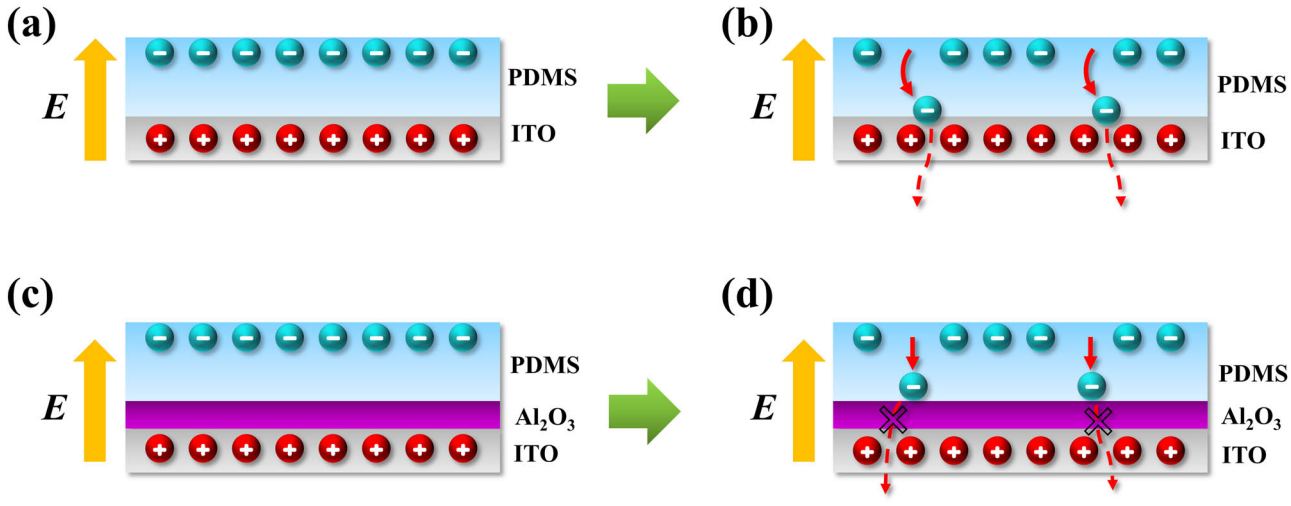

Figure 6: Working principle of the Al_2O_3 electron blocking layer. Schematic diagram of (a) the charge distribution and (b) electron drift process in the TENG without Al_2O_3. Schematic diagram of (c) the charge distribution and (d) the electron drift motion blocked by the Al_2O_3 layer in the TENG with an inserted Al_2O_3 layer.

caused by the electric field and a diffusion process caused by the concentration gradient of electrons [24]. Since the electric field intensity generated by the electrostatic induction is large, the electron diffusion transfer is comparably negligible. Therefore, in Figure 6b, only the drift motion is considered. Although the number of actually drifted electrons are not large due to the fact that the PDMS is an insulator, some electrons do have high enough energy to climb over the lowest unoccupied molecular orbital (LUMO) level of the PDMS (equivalent to the conduction band bottom of an insulator). These hot electrons eventually reach the bottom of the PDMS and escape from the bottom electrode, leading to the attenuation of the triboelectric charge stored in the friction layer. This reduces the output performance of TENG. However, the band gap of Al_2O_3 is wider than the highest occupied molecular orbital (HOMO)–LUMO gap of PDMS [25–27]. Therefore, after the introduction of Al_2O_3, it blocks the hot electrons, suppressing the charge transport. That is, the Al_2O_3 can effectively prevent the electrons from escaping at the bottom of PDMS, thereby improving the triboelectric charge storage capacity (see Figures 6c and d). We have measured the breakdown field of the CLD-Al_2O_3 thin film to be about 1.74 MV/cm, as shown in Figure 3d. In this measurement, a 23 nm Al_2O_3 film was sandwiched between two parallel electrodes. This breakdown field value is in the same order as that of the standard Al_2O_3 [28]. Today, in TENG community, to enhance the device output performance, most research has focused on the surface optimization of the surface friction layer [29–32]. However, these approaches yield little contributions toward the performance gain in long-term operation when surface modification/engineering is inevitably physically worn out by intimate contact and friction between the triboelectric materials [33]. Different from that strategy, the Al_2O_3 electron blocking layer here is located far away from the friction layer surface. Therefore, the resulted enhancement would not diminish even after the friction layer surface was worn during long-term operation. In addition, instead of competing with other methods, our technique could actually complement them. It is generic and could be applied in combination with other methods.

3.3 Growth mechanism of the CLD-Al_2O_3

Comparing with other more conventional Al_2O_3 deposition methods, the CLD technique may achieve the similar material quality while using cheaper and more convenient setup that does not rely on vacuum systems. Especially, the deposition temperature of CLD is much lower than other methods (see Table 1). Therefore, unless the substrate is sensitive to the aqueous environment, CLD could be used as a facile method to grow aluminum oxide thin films on electron devices. Nevertheless, an interesting question remains to be solved. That is, the deposition mechanism is yet to be unveiled. We propose the CLD-Al_2O_3 thin film growth mechanism as follows. First, owing to the abundance of OH groups in the growth liquid, OH are decorated onto the surface of substrate. Then, the OH groups and the $Al(OH)_3$ clusters undergo a continuous dehydration and polymerization, which result in the CLD-Al_2O_3 particle and subsequently thin film deposition. However, what is the status of the precursor? Are the $Al(OH)_3$ in ionic form, i.e., Al^{3+} and OH^-, like in a solution, or are they already forming colloids? To clarify this, we have let a laser beam pass through a 1:1 diluted liquid (see step 3 in Section 2.1 and Figure 1a). In a dark room, observing from the side, a bright "light path" of the incident light travelling in the liquid can be vividly seen, i.e., the Tyndall effect, as shown in Figure 3e. Therefore, some Al$(OH)_3$ colloids are already formed in the liquid in step 3 (see Section 2.1) before the deposition. Nevertheless, we note that our CLD method is fundamentally different from the existing sol–gel method and should not be mixed up. CLD has the advantage that a solid film can be directly grown on the surface of the sample in the growth liquid, and postannealing is not mandatory in the

Table 1: Comparison of different traditional Al_2O_3 deposition methods with CLD

No.	Method	Deposition temperature [°C]	Deposition rate [nm/min]	RMS [nm]	Breakdown field [MV/cm]	Ref.
1	CLD	25	0.17–0.25	~0.07	1.74	This work
2	ALD	180	~0.25 nm/cycle	0.1–1	~1	[12]
3	PECVD	800	~200	2.4–8	—	[13]
4	Sputtering	500	~5	—	—	[11]
5	Evaporation	65	24	—	1	[10]

process flow. If needed, however, postannealing could be used to increase the crystallinity of the film. On the contrary, the sol–gel method usually requires a plurality of heat treatments in the process of preparing the sol. After immersing the substrate in the sol, no film is formed in situ. Taking the sample out of the sol, a solid film is produced only after the high-temperature annealing, which is not an optional procedure. Therefore, the CLD method is intrinsically a room temperature process that accomplishes thin film deposition already in the growth liquid, which is not possible using the sol–gel method. The growth is in essence a pH-controlled condensation process of colloidal nanoparticles. No matter we put in a substrate or not, the condensation will anyway take place and that is why the liquid gradually becomes turbid. When a substrate is immersed in the growth liquid, the nanoparticles will nucleate on its surface and growth into a thin film. The particles are so fine that the film is rather flat and pin hole free. Of course, it is suitable for conformal coating of ultrathin films. Eventually, when the nanoparticles are exhausted, the liquid losses its ability to grow films. Actually, the growth already essentially stops when the colloidal particles become too large to be adsorbed. Note that our experiments do not exclude the growth from single ions. Although the liquid is proved to contain $Al(OH)_3$ sol, since the chemical reaction (see equation (1)) is dynamically taking place, it does not exclude the possibility that single $Al(OH)_3$ particles coming from the hydrolysis of single Al^{3+} ions can be directly incorporated into the thin film (without forming nanoparticles). Therefore, the CLD of Al_2O_3 is a complicated procedure involving $Al(OH)_3$ formation at both nanometer and single-ion level. With the growth mechanism revealed, one could specifically select chemical reactions that generate colloids, which can be condensed in a controlled fashion to grow the needed thin films in a facile manner. It opens the gateway to the synthesis of a bunch of functional films.

4 Conclusions

In summary, Al_2O_3 thin films were deposited on substrates by using the CLD method, which is a facile and low-cost method. The growth conditions are carefully optimized. The CLD method can grow large area thin films at room temperature with a reasonably good material quality suitable for electronic applications. The results show that the surface of the Al_2O_3 films is very flat. The breakdown field strength can reach 1.74 MV/cm. We have applied the as-grown Al_2O_3 films as the electron blocking layer of TENG, which provides a simple, low-cost, and effective method for improving the output performance of TENG. The open-circuit voltage and short-circuit current of the Al_2O_3-TENG is about 2.6 and 3 times, respectively, that of the Al_2O_3-free TENG. Finally, the growth mechanism is confirmed to include a pH-controlled colloidal condensation procedure, which could be used as the guideline to design the CLD of other thin films.

Acknowledgments: The authors gratefully acknowledge the help in measurement from Fujian Zhaoyuan Photoelectric Co., Ltd. and the financial support from National Natural Science Foundation of China (11674016).

Conflict of interest: The authors declare no conflict of interest regarding the publication of this paper.

References

[1] Abbott RA, Kamins TI. Sodium migration through electron-gun evaporated Al_2O_3 and double layer Al_2O_3 SiO_2 structures. Solid State Electron. 1970;13:565–76.
[2] Robertson J. High dielectric constant oxides. Eur Phys J Appl Phys. 2004;28:265–91.
[3] Shang Y, Zhong C, Jia R, Xiong H, Li H, Li X, et al. Preparation of low-permittivity K_2O–B_2O_3–SiO_2–Al_2O_3 composites without the addition of glass. Nanotechnol Rev. 2019;8:459–66.
[4] Zaininger KH, Waxman AS. Radiation resistance of Al_2O_3 MOS devices. IEEE Trans Electron Dev. 1969;16:333–8.
[5] Jo YJ, Jin HS, Ha MW, Park TJ. Sulfur incorporation at interface between atomic-layer-deposited Al_2O_3 thin film and AlGaN/GaN heterostructure. Electron Mater Lett. 2019;15:179–85.
[6] Zhang X, Zhang Y, Tian B, Jia Y, Liu Y, Song K, et al. Cr effects on the electrical contact properties of the Al_2O_3-Cu/15W composites. Nanotechnol Rev. 2019;8:128–35.
[7] Lee J, Kim JH, Im S. Pentacene thin-film transistors with Al_2O_{3+x} gate dielectric films deposited on indium-tin-oxide glass. Appl Phys Lett. 2003;83:2689–91.
[8] Nam Y, Lindvall N, Sun J, Park YW, Yurgens A. Graphene p–n–p junctions controlled by local gates made of naturally oxidized thin aluminium films. Carbon. 2006;50:1987–92.
[9] Saraie J, Ngan SF. Photo-CVD of Al_2O_3 thin films. Jan J Appl Phys. 1990;29:L1877.
[10] Shamala KS, Murthy LCS, Rao KN. Studies on optical and dielectric properties of Al_2O_3 thin films prepared by electron beam evaporation and spray pyrolysis method. Mater Sci Eng B. 2004;106:269–74.
[11] Musil J, Blažek J, Zeman P, Prokšová Š, Šašek M, Čerstvý R. Thermal stability of alumina thin films containing γ-Al_2O_3

phase prepared by reactive magnetron sputtering. Appl Surf Sci. 2010;257:1058–62.
[12] Ghiraldelli E, Pelosi C, Gombia E, Chiavarotti G, Vanzetti L. ALD growth, thermal treatments and characterisation of Al_2O_3 layers. Thin Solid Films. 2008;517:434–6.
[13] Cibert C, Hidalgo H, Champeaux C, Tristant P, Tixier C, Desmaison J, et al. Properties of aluminum oxide thin films deposited by pulsed laser deposition and plasma enhanced chemical vapor deposition. Thin Solid Films. 2008;516:1290–6.
[14] Fan FR, Tian ZQ, Wang ZL. Flexible triboelectric generator. Nano Energy. 2012;1:328–34.
[15] Wu C, Kim TW, Park JH, An H, Shao J, Chen X, et al. Enhanced triboelectric nanogenerators based on MoS_2 monolayer nanocomposites acting as electron-acceptor layers. ACS Nano. 2017;11:8356–63.
[16] Xu L, Wu H, Yao G, Chen L, Yang X, Chen B, et al. Giant voltage enhancement via triboelectric charge supplement channel for self-powered electroadhesion. ACS Nano. 2018;12:10262–71.
[17] Mallineni SSK, Behlow H, Podila R, Rao AM. A low-cost approach for measuring electrical load currents in triboelectric nanogenerators. Nanotechnol Rev. 2018;7:149–56.
[18] Wu C, Wang AC, Ding W, Guo H, Wang ZL. Triboelectric nanogenerator: a foundation of the energy for the new era. Adv Energy Mater. 2019;9:1802906.
[19] Shang ZW, Hsu HH, Zheng ZW, Cheng CH. Progress and challenges in p-type oxide-based thin film transistors. Nanotechnol Rev. 2019;8:422–43.
[20] Feng J, Kriechbaum M, Liu LE. In situ capabilities of small angle x-ray scattering. Nanotechnol Rev. 2019;8:352–69.
[21] JCPDS File NO. 46-1212. JCPDS-International Center for Diffraction Data. ICDD; 2001.
[22] Nayak PK, Hedhili MN, Cha D, Alshareef HN. High performance In_2O_3 thin film transistors using chemically derived aluminum oxide dielectric. Appl Phys Lett. 2013;103:033518.
[23] Brand JVD, Sloof WG, Terryn H, De Wit JHW. Correlation between hydroxyl fraction and O/Al atomic ratio as determined from XPS spectra of aluminium oxide layers. Surf Interface Anal. 2004;36:81–88.
[24] Cui N, Gu L, Lei Y, Liu J, Qin Y, Ma X, et al. Dynamic behavior of the triboelectric charges and structural optimization of the friction layer for a triboelectric nanogenerator. ACS Nano. 2016;10:6131–8.
[25] Wang B, Huang W, Chi L, Al-Hashimi M, Marks TJ, Facchetti A. High-k gate dielectrics for emerging flexible and stretchable electronics. Chem Rev. 2018;118:5690–754.
[26] Zhao D, Liu Y, Zhang Q, Zhang Y, Zhang W, Duan Q, et al. Surface stress-based biosensor with stable conductive AuNPs network for biomolecules detection. Appl Surf Sci. 2019;491:443–50.
[27] Guo QZ, Yang LC, Wang RC, Liu CP. Tunable work function of $Mg_xZn_{1-x}O$ as a viable friction material for a triboelectric nanogenerator. ACS Appl Mater Interfaces. 2018;11:1420–5.
[28] Kolodzey J, Chowdhury EA, Adam TN, Qui G, Rau I, Olowolafe JO, et al. Electrical conduction and dielectric breakdown in aluminum oxide insulators on silicon. IEEE Trans Electron Dev. 2000;47:121–8.
[29] Ding P, Chen J, Farooq U, Zhao P, Soin N, Yu L, et al. Realizing the potential of polyethylene oxide as new positive tribomaterial: over 40 W/m^2 high power flat surface triboelectric nanogenerators. Nano Energy. 2018;46:63–72.
[30] Chen SN, Chen CH, Lin ZH, Tsao YH, Liu CP. On enhancing capability of tribocharge transfer of ZnO nanorod arrays by Sb doping for anomalous output performance improvement of triboelectric nanogenerators. Nano Energy. 2018;45:311–8.
[31] Wang S, Zi Y, Zhou YS, Li S, Fan F, Lin L, et al. Molecular surface functionalization to enhance the power output of triboelectric nanogenerators. J Mater Chem A. 2016;4:3728–34.
[32] Shin SH, Kwon YH, Kim YH. Triboelectric charging sequence induced by surface functionalization as a method to fabricate high performance triboelectric generators. ACS Nano. 2015;9:4621–7.
[33] Yu Y, Li Z, Wang Y, Gong S, Wang X. Sequential infiltration synthesis of doped polymer films with tunable electrical properties for efficient triboelectric nanogenerator development. Adv Mater. 2015;27:4938–44.